We are IntechOpen,
the world's leading publisher of
Open Access books
Built by scientists, for scientists

4,800
Open access books available

122,000
International authors and editors

135M
Downloads

154
Countries delivered to

Our authors are among the

TOP 1%
most cited scientists

12.2%
Contributors from top 500 universities

Interested in publishing with us?
Contact book.department@intechopen.com

Numbers displayed above are based on latest data collected.
For more information visit www.intechopen.com

Optical Absorption and Thermal Effects of Plasmonic Nanostructures

Jingzhi Wu and Yanhong Wang

Additional information is available at the end of the chapter

Abstract

With resonant light illumination, metallic nanostructures convert electromagnetic fields' energy into heat because of optical absorption associated with plasmonic resonance. The optical absorption triggers a heat generation process that involves not only the absorption of photon energy but also heat transfer from the nanostructures to the surrounding medium. In this chapter, we study enhanced optical absorption of plasmonic nanostructures. Moreover, thermal effects induced by optical absorption and heat transfer between nanostructures are analyzed.

Keywords: plasmonics, nanoparticle, thermal effect, absorption, optical trapping

1. Introduction

Optically excited nanostructures have large absorption cross-sections, which lead to efficient heat generation. Strength and localization of heat generation strongly depend on geometry and composition of plasmonic nanostructures [1, 2]. The regimes of optical heating of nanostructures can be collective or local. The collective heating is realized in a large and dense ensemble of nanoparticles (NPs) where heat fluxes from individual NPs add up, leading to high-temperature distribution [3]. The collective heating is typically realized in the regime of continuous wave (CW) illumination when the system has enough time to reach a non-equilibrium steady state with increased temperature [4, 5]. The local regime of heat generation can produce high temperature in confined volumes within or in the vicinity of a plasmonic nanostructure. The local and collective heating mechanisms depend on the composition and dimensions of nanostructures [6, 7]. Moreover, the temperature distribution and the efficiency of temperature generation depend on the shape of nanostructure [8, 9].

INTECH
open science | open minds

The theoretical description of plasmonic photothermal effect can be modelled as: the light scattering/absorption, the subsequent heat generation, and heat dissipation or transfer in the system of nanostructures [10–12]. The laser-induced heat generation and conduction in arbitrary plasmonic structures can be numerically modelled and solved, using methods as finite element method (FEM) [13], discrete dipole approximation (DDA) [14], boundary element method (BEM) [15], or finite-difference time-domain (FDTD) [16]. Experimental methods have been developed for observing light-induced heating effects in plasmonic systems and characterizing the temperature increase of nanostructures. In time domain, transient thermo-reflectance technique (TTR) was used to measure the pulsed-laser heating of a metal film by a pump-probe setup, with sub-picosecond resolution [17–19]. In a spatial domain, the development of scanning thermal microscope (SThM) enables thermal microscopic imaging with sub-500-nm resolution [20]. Other thermal microscopic imaging methods were also demonstrated, such as measuring the phosphor decay time [21], phase transition of organic molecules [22], or electric conductance of metal thin film [23].

In this chapter, the optical absorption of metallic nanostructures is simulated by finite element method. Enhanced optical absorption is demonstrated by designing periodic and random nanostructures. Broadband optical absorption is achieved based on refractory plasmonic nanostructures for high-temperature applications. Experiments show that optical absorption of 90% in the wavelength range from 200 to 1100 nm can be achieved using random nanostructures. The temperature distribution of NPs solution is measured using polarization anisotropy of fluorescence (FPA). The heat transfer between nanostructures in different surrounding media is analyzed using heat transfer theory. Thermal force induced by temperature gradient in the surrounding aqueous medium is also discussed. Nanoparticle trapping using both optical force and thermal force is demonstrated.

2. Optical absorption of plasmonic nanostructures

2.1. Plasmonic materials

Plasmonic materials are typically metals. Plasmonic resonance occurs when an electromagnetic radiation of a well-defined wavelength interacts with a metallic system: free electrons in the conduction band will oscillate with respect to fixed positive ions. When the exciting field is resonant with the electron oscillation frequency, a strong electromagnetic field develops near the nanostructure surface. The optical properties of noble metals can be described by a complex dielectric function ε_M that depends on the frequency of the incident light ω. There are two major contributions to ε_M: (1) the quasi-free movement of the conduction band electrons induced by the incident radiation and (2) the electronic interband transitions that may take place if the energy of photons exceeds the energy between energy bands. The dielectric function containing both contributions can be described by the Drude–Lorentz model [24]:

$$\varepsilon_M(\omega) = \varepsilon_r - \sum_j \frac{\omega_{Pj}^2}{\omega^2 + i\gamma_j\omega} + \sum_j \frac{\Delta\varepsilon_j\Omega_{Pj}^2}{\Omega_{Pj}^2 - \omega^2 - i\Gamma_j\omega} \tag{1}$$

where ε_r describes the optical response at high frequencies, which includes the background dielectric function of the ionic cores, γ is the characteristic collision rate responsible for

damping of electron oscillations that related to energy losses by heating and ω_p is the volume plasma frequency of the free electron system defined as: $\omega_P = \sqrt{ne^2/\varepsilon_0}$, where e is the elementary charge, ε_0 is the permittivity of free space and m is the electron mass. $\Delta\varepsilon_j$ is the contribution of interband transition to the dielectric function and Ω_p and γ are the plasma and damping frequencies for the bound electrons, respectively. The inclusion of more terms (j) in the sum provides a better fitting to the experimental data. The dielectric functions of commonly used metal materials gold (Au), silver (Ag) and one refractory material Tungsten (W) are shown in **Figure 1**.

Upon optical illumination, a nanostructure both absorbs and scatters light, which can be described by scattering, absorption and extinction cross-sections. Mie theory gives the exact analytical solution to the scattering and absorption of simple cases, for example, metallic spheres. Nevertheless, the scattering of particles with arbitrary shapes is beyond the ability of Mie solution. The calculation of the EM fields at all points in space when light interacts with a nanostructure of arbitrary shapes and dielectric properties is a complex problem that needs to be solved numerically. Several numerical methods, such as FDTD, DDA and FEM, are suitable for obtaining the scattering/absorption of nanostructures with arbitrary shapes. In this work, we use FDTD method for the numerical calculation of the scattering/absorption spectra of various plasmonic nanostructures.
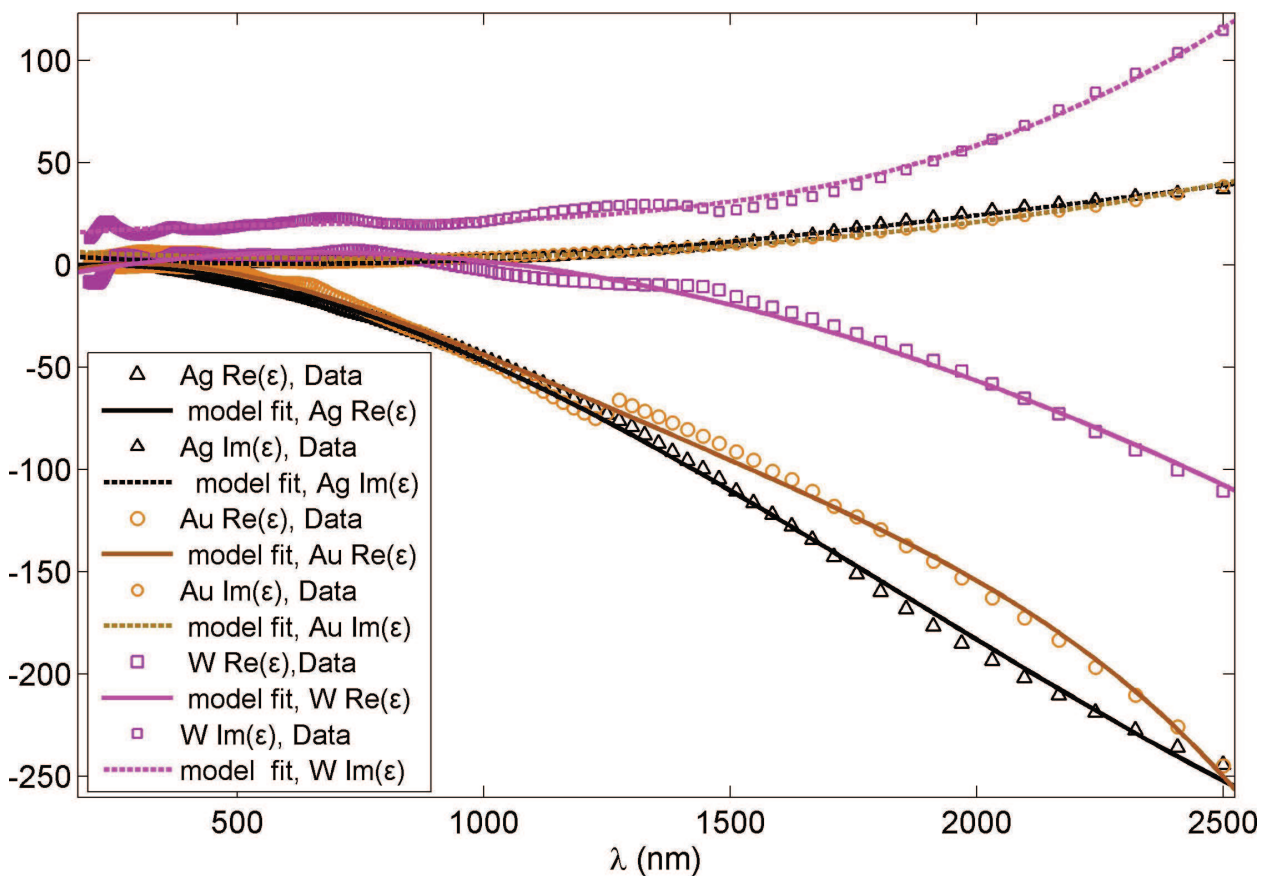

Figure 1. Dielectric function of metals.

Recent experimental findings show that the imaginary part of the dielectric function changes significantly with the increasing temperature [25], whereas the real part remains almost intact. The temperature-dependent deviations in the gold optical constants are quite significant. A temperature dependent non-linear permittivity model combining several oscillators (j) with lifetime Γ_j, strength f_j and frequency ω_j has been proposed recently [26]. Its expression comprises two terms: the first one taking into account the conduction electrons and the influence of temperature and the second one expressing the interband absorptions:

$$\varepsilon_M(\omega) = 1 - \frac{\Omega_P(T)^2}{\omega^2 - i\eta\omega\tilde{\Gamma}(T)} + \sum_j \frac{f_j\omega_P^2}{\omega_j^2 - \omega^2 + i\Gamma_j\omega} \tag{2}$$

$$\Omega_P(T) = \frac{\Omega_P}{\sqrt{1 + 3\zeta(T - T_0)}} \tag{3}$$

$$\tilde{\Gamma}(T) = \Gamma_0 + \Gamma(T) - \Gamma(T_0) \tag{4}$$

where $\Gamma(T)$ is the total damping coefficient at temperature T, γ_0 is the interband damping coefficient. $\Omega_P = \sqrt{f_D\omega_P}$ is the modified plasma frequency including the oscillator strength f_0. ζ is the thermal expansion coefficient and η is a dimensionless parameter that can be tuned to take into account defects-induced damping changes.

Temperature change can strongly modify the field enhancement and absorption characteristics of plasmonic devices. A deep understanding of the temperature dependence of the optical and thermal phenomena in plasmonic structures has a great importance in a variety of research areas, including plasmonics and near-field irradiative heat transfer. The increase in the imaginary part at elevated temperatures significantly reduces the surface plasmon polariton propagation length and the quality factor of the localized surface plasmon resonance. Even though the optical properties of bulk metals at elevated temperatures have been studied, the temperature-dependent data for plasmonic materials is still largely missing. Further experiments and analytical models need to be developed for accurate modelling of high-temperature plasmonic devices operating in a steady or dynamic state.

2.2. Broadband absorption

Enhancing light absorption of plasmonic materials has evoked great interest of researchers in many fields of thermophotovoltaics and solar thermal applications. One of the approaches to improve the absorbing performance is to utilize micro/nanostructures on material surface to produce unique optical characteristics that facilitate a route to achieving spectrum selectivity [27].

Applications in the high-temperature fields strongly demand for improving optical performances of refractory materials. The absorption wavelength of an ideal absorber is from 400 to 1500 nm for maximum absorption of the solar spectrum. This absorption spectrum selectivity is required to prevent re-radiation of the absorbed energy. It is possible to limit re-radiation by heating the material above 1200°C to match the narrow bandgap of photovoltaic cells [28]. In

order to obtain desired optical properties, different micro/nanostructures on refractory materials supporting plasmonic resonance have been proposed.

2.2.1. Periodic plasmonic structures

First, we study the absorption enhancement and spectrum selectivity of refractory material (Tungsten, W) with periodic structures comprising cylinder array. The incident light is a plane wave with wavelength range from 400 to 2500 nm. The material property is modelled to fit experimental data from the literature using a Drude-Lorentz model.

From **Figure 2**, we can see that the absorption enhancement can be achieved by adjusting the structure parameters of nanostructures in visible and near-infrared wavelength range. However, absorption enhancement is not obvious at a longer wavelength (> 2000 nm) because plasmonic resonance cannot be excited.
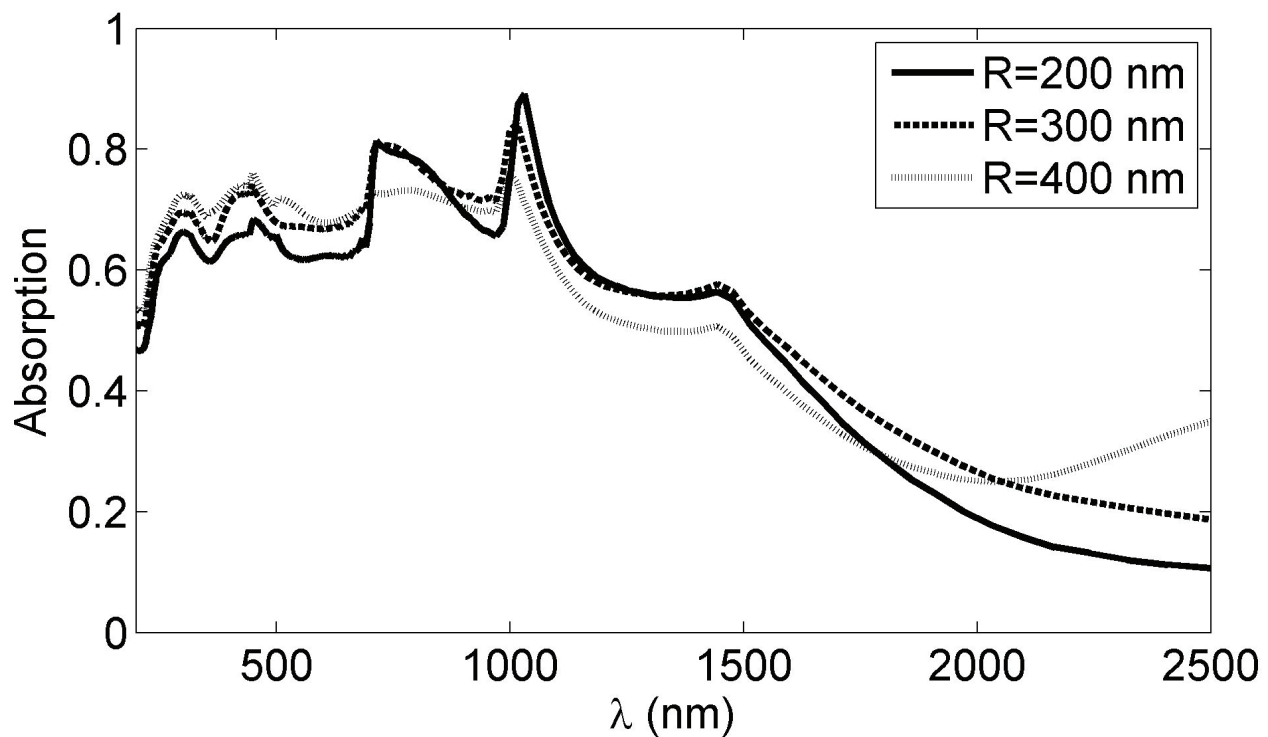

Figure 2. Absorption of the periodic plasmonic cylinders with different radii R, with P = 1000 nm and H = 500 nm. Inset is the model of periodic array of plasmonic cylinders with period P, height H and radius R.

Figure 3 shows that the absorption peak wavelength is dependent on the structure period. However, the absorption is gradually decreasing for the larger period because of weak plasmonic coupling between periodic structures. It is difficult to excite plasmonic resonance modes beyond the wavelength of 1200 nm. Therefore, there is no resonance peak in the mid-infrared range for achieving the spectrum selectivity absorption to match the narrow bandgap of photovoltaic cells.

The absorption of periodic structures with different height is shown in **Figure 4**. It shows that the absorption peak wavelength is strongly affected by the height of surface structure. Increasing the
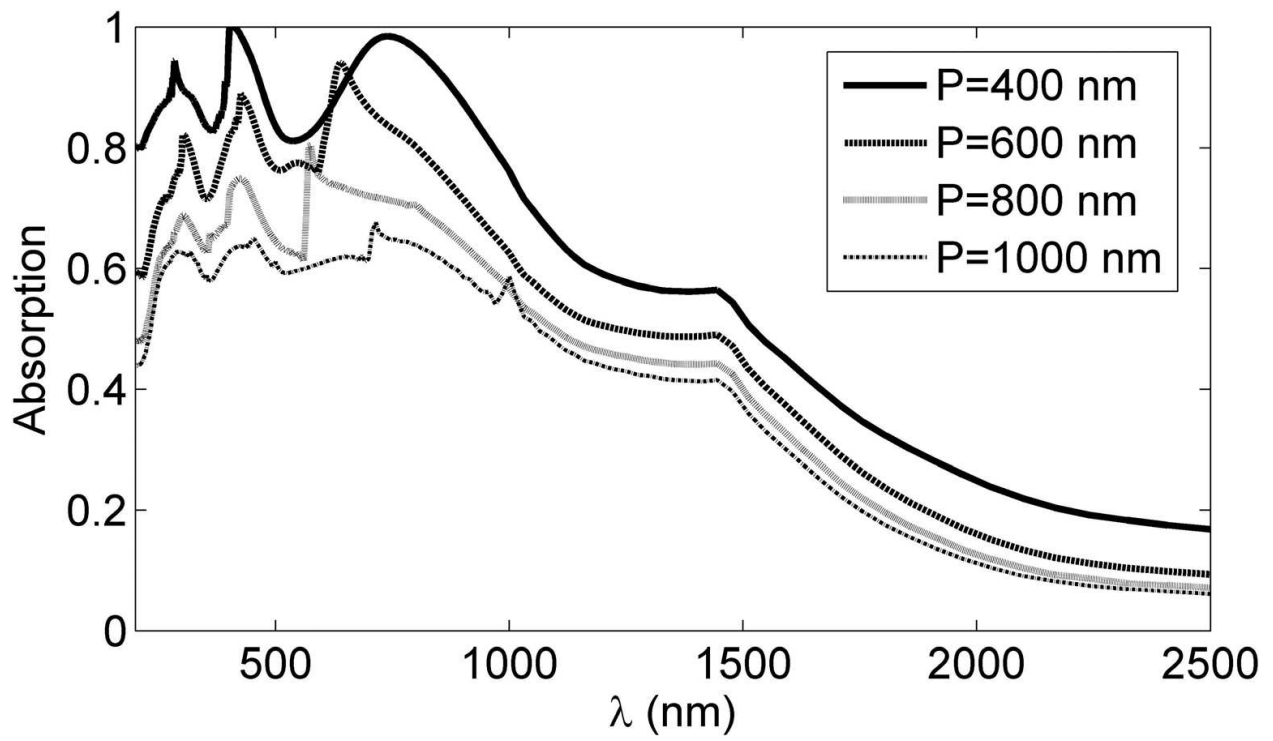
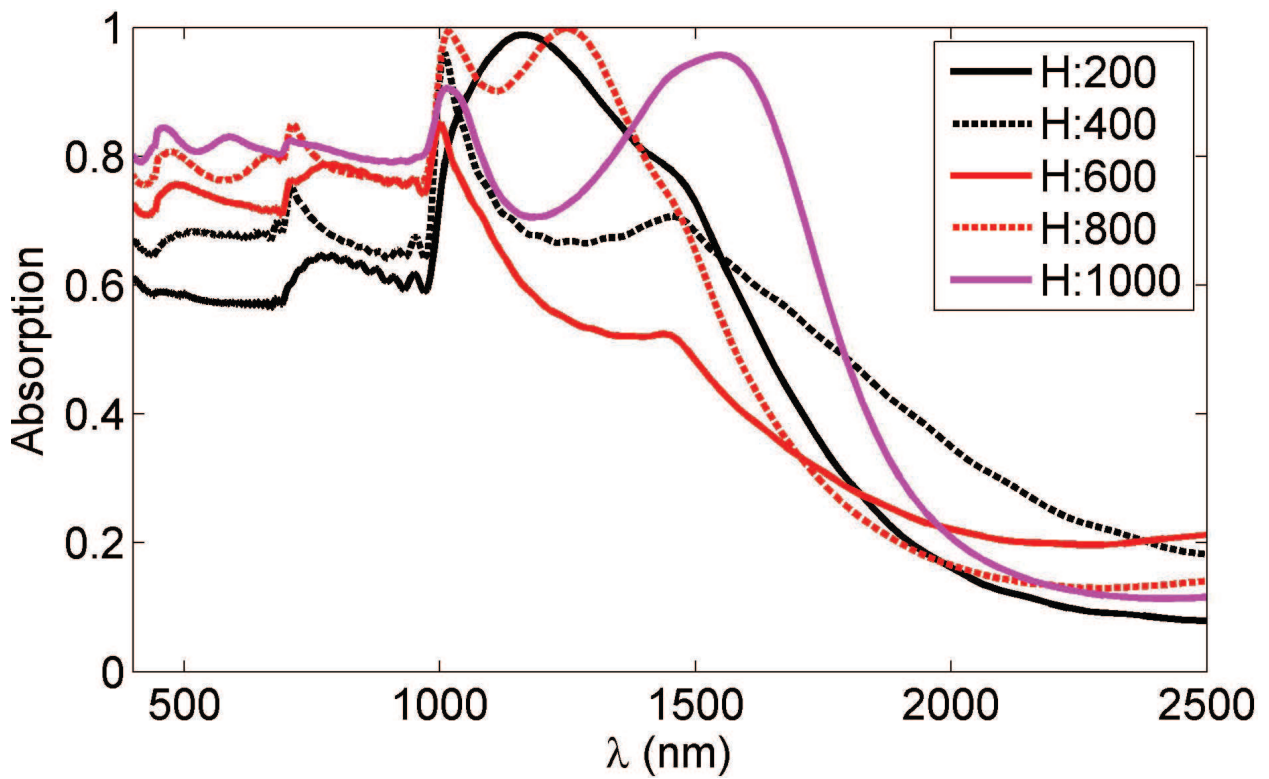**Figure 3.** Absorption of the periodic structures with different period at R = 100 nm and H = 500 nm.

Figure 4. Absorption of the periodic structures with different heights at R = 300 nm and P = 1000 nm.

height of structures can enhance absorption efficiency as new resonant modes are supported. For instance, the absorption is greatly enhanced at wavelength 1500 nm for the structure with H = 1000 nm. Varying the height of structure can also shift the peak absorption wavelength, for example, the peak absorption is shifted to 1200 nm for the structure with H = 800 nm.

2.2.2. Random plasmonic structures

While optical absorption of periodic structures can be precisely controlled, random structures offer flexibility to design and fabricate. Random structures can be described by their height distribution and correlation function. There is an important statistical height parameter to be often used, root mean square (RMS) R_q, for evaluating the amplitude of surface roughness. The correlation length usually describes lateral dimensions and is another spatial parameter which is used for the determination of peak density corresponding to lateral dimensions [29].

The random structure is characterized by a specified RMS (R_q) and correlation length (L_c), which are related to the correlation function by [30]:

$$\langle H(\vec{r})H(\vec{r} + \vec{\delta})\rangle = R_q^2 \exp\left(-\left(\frac{\delta}{L_c}\right)^2\right) \tag{5}$$

where δ is the sampling resolution of the surface.

$$R_q^2 = \frac{1}{L}\int_0^L \left(z(x)^2\right)dx \tag{6}$$

Here, L is the sample length of the profile and z(x) is the profile heights measured from a reference line. For convenience, the reference line is defined as x-axis along the lateral surface.

For the following FDTD simulations, the random surface roughness is generated by creating a matrix of uniform random numbers in k-space [31]. First, generating a square two-dimensional random rough surface F(x,y) with N×N surface points. The surface has a Gaussian height distribution and exponential auto covariance functions (in both x and y). L_S is the length of the surface side. Assuming $L_{cx} = L_{cy} = L_c$ are the correlation lengths in x and y, a Gaussian filter is applied to this matrix to remove high-frequency components and then a Fourier transform is used to transform the matrix back to real space.

Figure 5 shows the absorption of random structures with different RMS values. The correlation length (Lc) of each structure is set as 0.5 µm. We can see that absorption efficiencies are above 80% in the wavelength range of 400 to 1500 nm when RMS values are larger than 0.3 µm. For longer wavelength range > 1500 nm, the absorption efficiency is strongly dependent upon the value of RMS. Strong resonance peaks can be excited near 2 µm for the structure with RMS > 0.3 µm. The resonance peak (marked by red circles in **Figure 5**) obviously shifts toward longer wavelength for bigger RMS values. The overall absorption efficiency at off-resonance peak wavelength is sharply decreased. This property is beneficial for engineering spectrum selectivity in the mid-infrared wavelength range by adjusting the RMS parameter.
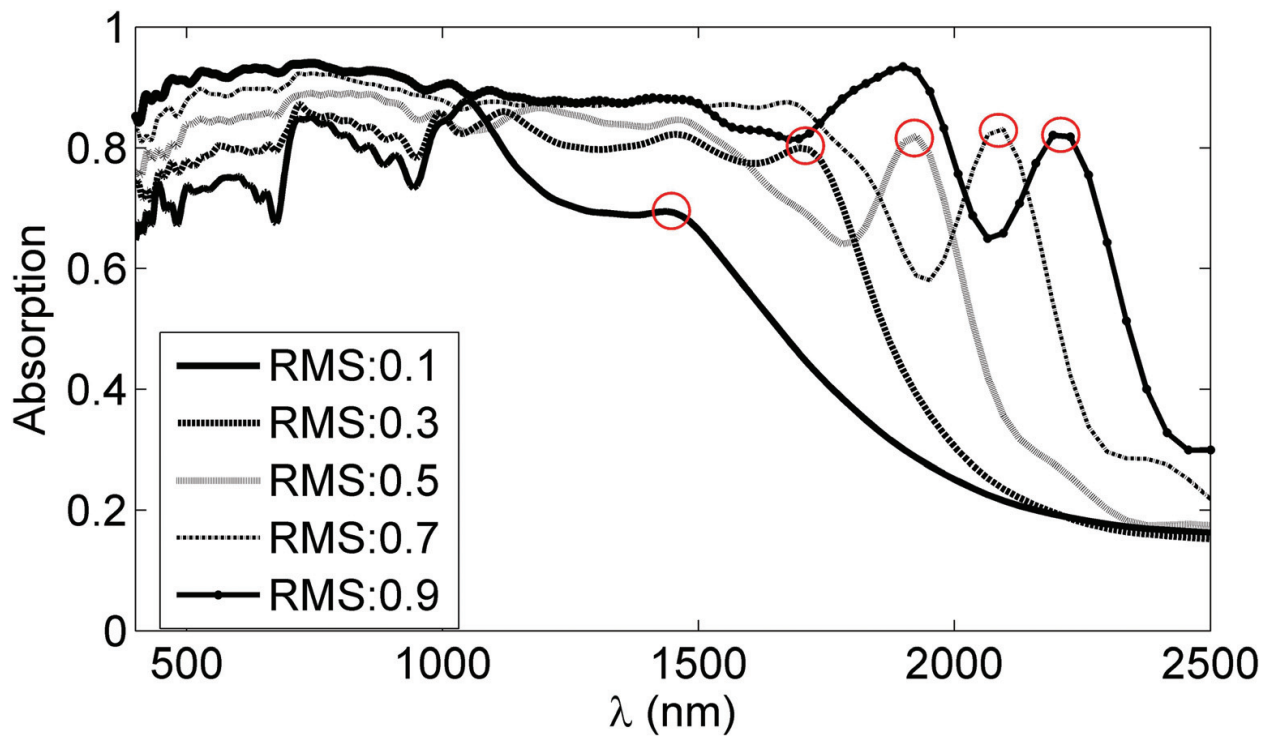
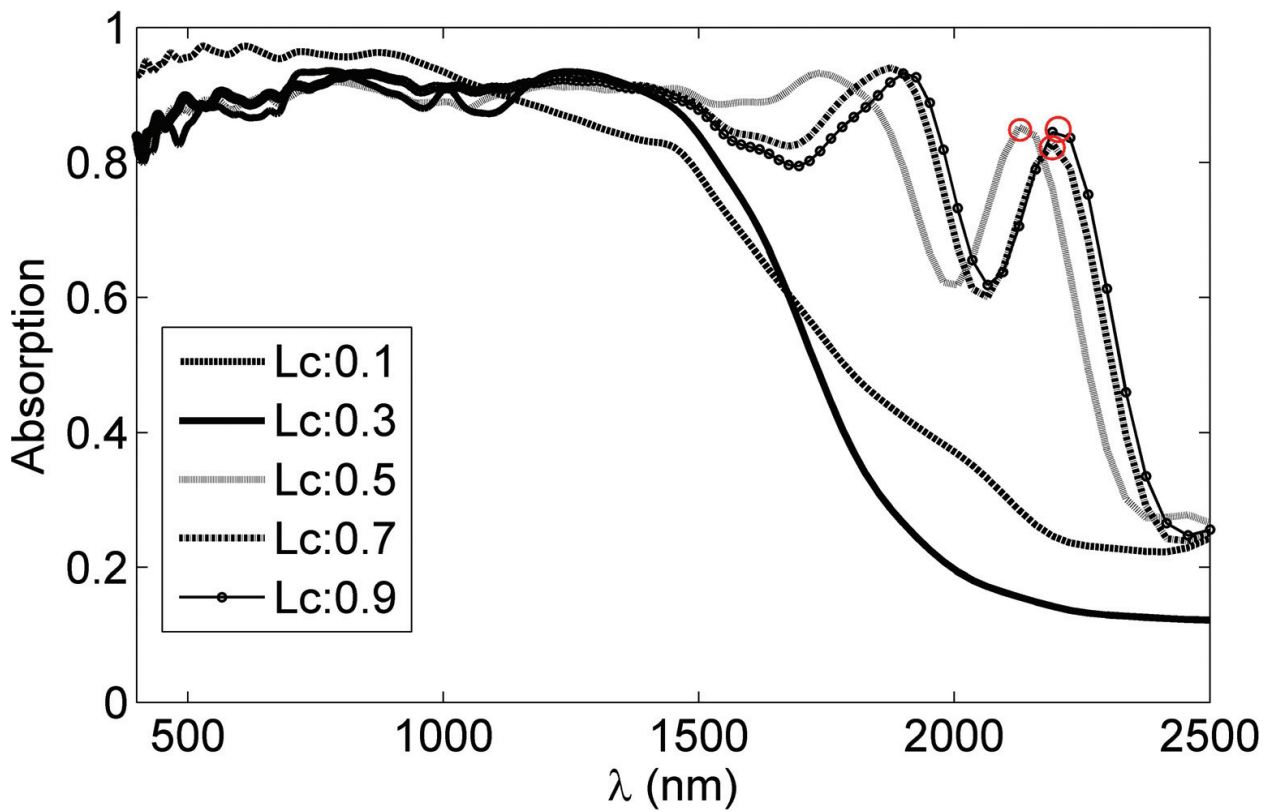**Figure 5.** Absorption of random structures with various RMS values at Lc = 0.5 μm.

Figure 6. Absorption of random structures with different Lc values at RMS = 0.7 μm.

The optical absorption of structures with a different correlation length Lc and same RMS (0.7 μm) is plotted in **Figure 6**. It can be seen that the absorption efficiency is over 80% in the wavelength range from 400 to 1500 nm. However, the value of Lc has a much stronger effect on the absorption in the wavelength range from 1.5 to 2.5 μm. New resonance peaks with strong absorption are excited at Lc is equal to 0.5, 0.7 and 0.9 μm, but the resonance peaks are not obviously shifted with different Lc values (such as the positions marked by red circles in **Figure 6**). The absorption enhancement spectrum can be gradually broadened to 2 μm when Lc is 0.7 μm. Therefore, absorption enhancement and spectrum selectivity of refractory materials can be obtained by controlling RMS and Lc of the random structures.

To demonstrate the absorption enhancement, random nanostructures have been fabricated using femtosecond (fs) laser on the tungsten substrate (**Figure 7**). The optical absorption spectrum measured by a spectrophotometer shows that the absorption efficiency of nanostructures with RMS of 0.8 μm is greater than 90 % in the wavelength range from 200 to 1100 nm. However, the sample with surface structure RMS of 0.08 μm (polished surface) has much lower absorption (less than 70 % for $\lambda > 600$ nm). It indicates that the optical absorption of the refractory material depends on the size of microstructures on the surface.
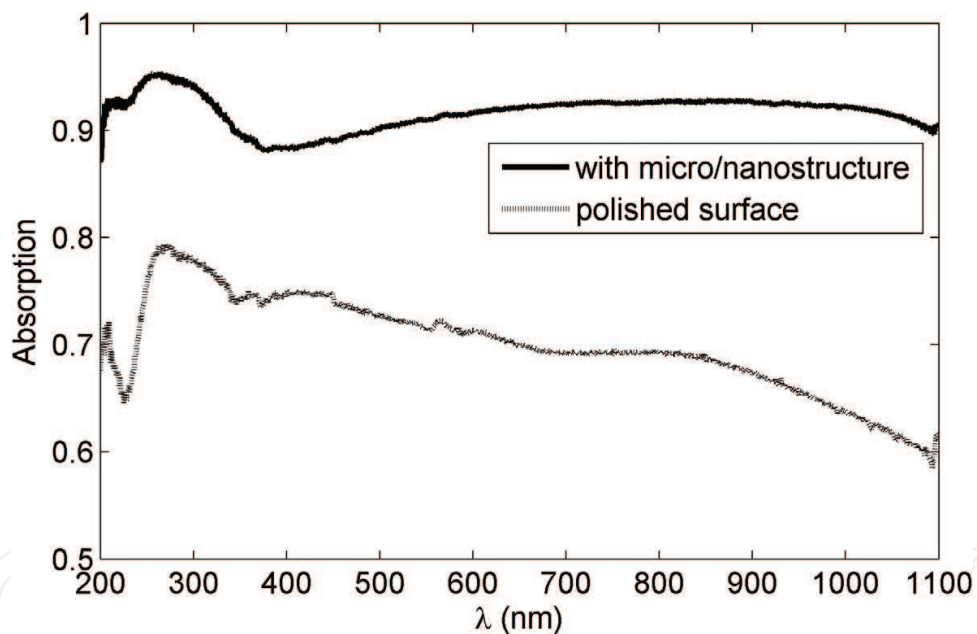

Figure 7. Absorption spectrum of laser-processed tungsten samples with RMS of 0.8 μm and polished surface with RMS of 0.08 μm. Inset shows the sample with polished surface (left) and the sample with micro/nanostructure (right).

3. Thermal effects of plasmonic resonance

The loss of metals, which is manifested by the imaginary part of permittivity $Im(\varepsilon_M)$, implies that resistive heat will be generated while illuminated by EM fields. A large portion of the energy of incident photons is transferred to the energy of the collective oscillation of excited electrons within the nanostructure. Plasmonic nanostructures show strong scattering and absorption of

light at specific wavelength in visible and near-infrared regions because of plasmonic resonances. Associated with the absorption of optical radiation is the generation of heat, which originates from non-radiative decay due to electron–electron and electron–photon interactions. Based on the Joule heating effect, the heat power volume density q_p can be written as

$$q_P = \frac{1}{2}(\mathbf{J}^*\mathbf{E} + \mathbf{J}\mathbf{E}^*) = \varepsilon_0\omega\mathrm{Im}(\varepsilon_M)|\mathbf{E}|^2 \tag{7}$$

where $\mathbf{E}$ is the electric field in the nanostructure and $\mathbf{J}$ is the electric current density.

3.1. Localized temperature field

The resulting temperature distribution around a nanostructure is described by the heat transfer equation, a differential equation that must be solved numerically [32]:

$$\rho(\tilde{r})C_T(\tilde{r})\frac{\partial T(\tilde{r},t)}{\partial t} = \nabla\kappa(\tilde{r})\nabla T(\tilde{r},t) - q_P(\tilde{r},t) \tag{8}$$

here $\tilde{r}$ and t are the spatial coordinates, and time $T(\tilde{r}, t)$ is the local temperature, ρ, C_T and κ are the mass density, specific heat and thermal conductivity, respectively.

The time evolution of the temperatures T_i of N objects is governed by the following energy equations (i = 1,…,N) [33]:

$$\rho_i C_i V_i\frac{dT_i(t)}{dt} = Q_i^{abs}(t, T_1, \cdots, T_N, T_b) \tag{9}$$

here, the left-hand side is the time variation of the internal energy of object i, with ρ_i, C_i and V_i representing its mass density, heat capacity and volume, respectively.
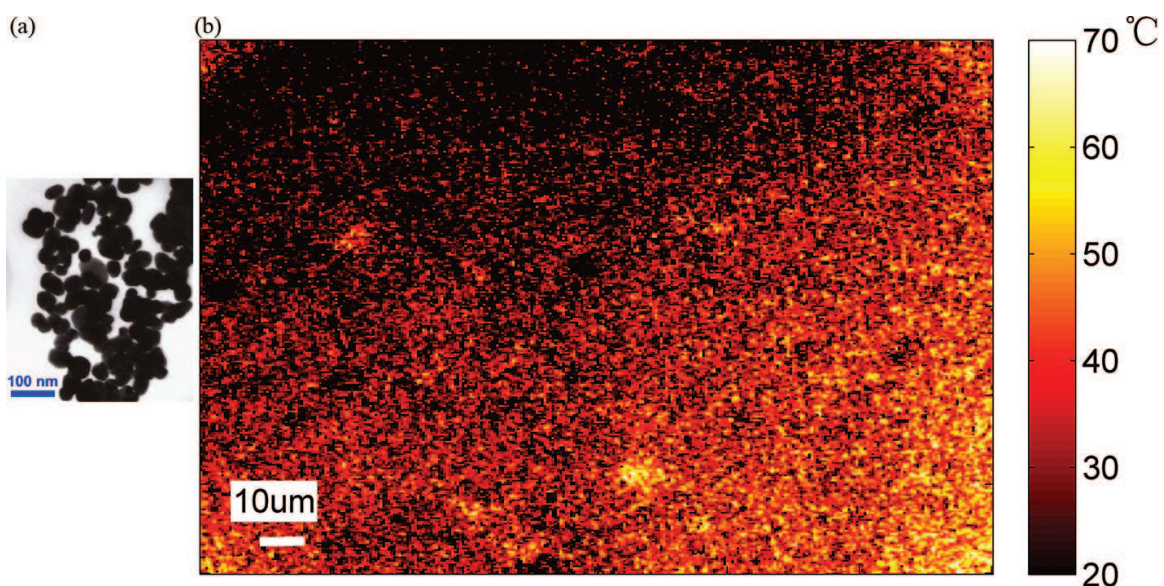

Figure 8. (a) The SEM image of Ag particles. (b) The temperature map of Ag particles in solution measured by FPA method.

Figure 8 shows the temperature increase of silver nanoparticles solution measured using fluorescence polarization anisotropy (FPA) method [34]. The FPA is directly related to rotational diffusion induced by molecular Brownian dynamics. In general, a population of fluorophores illuminated by linearly polarized incident light re-emits partially polarized fluorescence due to the random orientation of the molecules. By measuring the polarization anisotropy of fluorescence, the temperature field around the fluorophore molecules can be obtained.

3.2. Heat transfer between nanoparticles

Considering a collection of N objects located at positions r_i and maintained at different temperatures T_i with $i = 1, \cdots, N$, in a thermal bath with temperature fixed at T_b. Suppose there is no phase and mass change of materials and the size of these objects is small enough compared with the thermal wavelength $\lambda_T = \hbar c / k_B T$ (T is the temperature, c is the speed of light in vacuum, k_B is Boltzmann's constant and $\hbar$ is Plank's reduced constant), so that all individual objects can be modelled as radiating dipoles. According to fluctuation-dissipation theorem, the net heat transfer on particle i as a sum of exchanges with the other particles and with the thermal bath [35] is

$$Q_i^{abs}(t, T_1, \cdots, T_N, T_b) = \left\langle \frac{d\mathbf{p}_i(t)}{dt} \cdot \mathbf{E}(r_i, t) \right\rangle \tag{10}$$

where the dipole moment $\mathbf{p}_i(t)$ is composed of its fluctuating and induced part, the local field $\mathbf{E}$ is the sum of incident part $\mathbf{E}^b$ without scatters and its induced part $\mathbf{E}^{ind}$ omitting the frequency dependence. The net heat transfer can be rewritten as [36]:

$$Q_i^{abs}(t, T_1, \cdots, T_N, T_b) =$$
$$\int_0^{+\infty} \frac{d\omega}{2\pi} \hbar\omega \left[\sum_{j \neq i} \frac{4\chi_i\chi_j}{|\alpha_i|^2} n_{ji}(\omega) \text{Tr}(\text{T}_{ij}^{-1}\text{T}_{ij}^{-1*}) + \frac{4\chi_i k^2}{|\alpha_i|^2} n_{bi}(\omega) \sum_{jk} \alpha_j\alpha_k^* \text{Tr}\left(\text{T}_{ij}^{-1}\text{Im}(\text{G}_{jk}^0)\text{T}_{ki}^{-1*} \right) \right] \tag{11}$$

In the above equation, $\chi_j = \text{Im}(\alpha_j) - \frac{k^3}{6\pi}|\alpha_j|^2$, $n_{ij}(\omega) = n(\omega, T_i) - n(\omega, T_j)$, where $n(\omega, T) = 1/[\exp(\hbar\omega/k_B T) - 1]$ is the Bose-Einstein distribution. $\text{T}_{ij} = \delta_{ij}\text{I} - (1 - \delta_{ij})k^2\alpha_i\text{G}_{ij}^0$, G_{ij}^0 is the dyadic Green tensor in free space

$$\text{G}_{ij}^0 = \frac{\exp(ik\rho)}{4\pi\rho} \left[\left(1 + \frac{ik\rho - 1}{k^2\rho^2} \right)\text{I} + \frac{3(1 - ik\rho) - k^2\rho^2}{k^2\rho^2}\hat{\rho}\otimes\hat{\rho} \right] \tag{12}$$

here, $k = \omega/c$, $\hat{r} = r/r$, $\boldsymbol{\rho} = \mathbf{r'} - \mathbf{r}$, and $\rho = |\boldsymbol{\rho}|$.

The power dissipated inside the particle i at a given frequency ω by the fluctuating field E_{ij} generated by the particle j can be calculated from the work of the fluctuating EM field on the charge carriers as:

$$P_{j \to i} = 3 \int_0^\infty \frac{d\omega}{2\pi} \Theta(\omega, T_j) \Gamma_{i,j}(\omega) \tag{13}$$

where $\Gamma_{i,j}(\omega)$ is the transmission coefficient (TC)

$$\Gamma_{i,j}(\omega) = \frac{4}{3}\frac{\omega^4}{c^4}\mathrm{Im}(\alpha_i)\mathrm{Im}(\alpha_j)\mathrm{Tr}[G^{ij}G^{ij*}] \tag{14}$$

Here α_i is the particle's polarizability. G^{ij} is the dyadic Green tensor.

The heat flux (HF) is rewritten as

$$P_{j\to i} = 3\left(\frac{\pi^2 k_B^2 T}{3h}\right)\overline{\Gamma}_{i,j}\Delta T \tag{15}$$

$\pi^2 k_B^2 T/3h$ is universal quantum of thermal conductance. $\overline{\Gamma}_{i,j}$ is the mean transmission coeffi-
cient. $\overline{\Gamma}_{i,j} = \int dx f(x)\Gamma_{i,j}(x)/\int_0^\infty f(x)dx$, where $f(x) = x^2 e^x/(e^x - 1)^2$ is a function reminiscent of

the mean energy of a harmonic oscillator and $\int_0^\infty f(x)dx = \pi^2/3$.

Figure 9 shows the interparticle heat flux (HF) in a three-particle system (SiC particles)
between particles 1 and 2 with particle 3 in the middle [35]. The HF is normalized by the HF
between particles 1 and 2 without particle 3 in the same thermal conditions, for $R_2 = R_1$. It
shows that the HF mediated by the presence of the third particle can be significantly larger
than the value for two isolated dipoles. The enhancement of heat transfer can be over three
orders of magnitude for particles separated by distance over 200 nm. The heat transfer
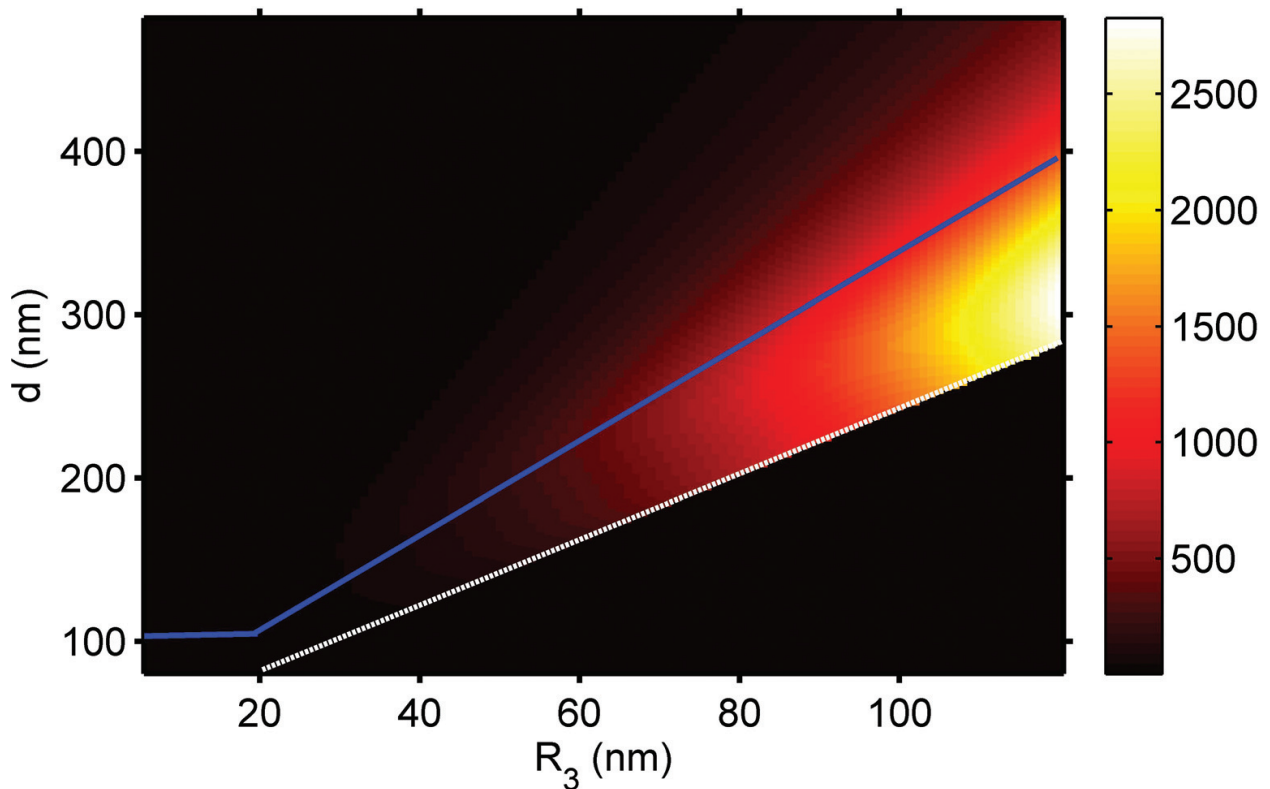between nanoparticles is strongly varied by the interactions with a third nanoparticle.

Figure 9. HF normalized to two-particle case with R2= R1. Normalized heat flux (HF) exchanged between particles 1 and
2 separated by different distances and particle 3 with various radii is located at the center in between. The white dashed
line is where three nanoparticles are touching. The blue line is distance d–R1–R2–2R3 = max (R1,R2,R3) [35].

3.3. Thermal driving force

When colloidal particles in solutions are exposed to a temperature gradient, they are subjected to thermophoretic forces, which drive them toward one side of the gradient. The direction of particle movement depends on the ambient temperature and the details of particle solvent interactions. Despite much data available, the physical mechanisms of thermophoresis and the thermal driving force in liquids are not well understood. Particle motion in non-uniform gases is well described by kinetic theory. However, surface forces are essential in aqueous solutions; therefore, the steady state has to be characterized in terms of the mechanical equilibrium of hydrodynamic stress and surface forces.

The probability density distribution $p(r)$ for finding the particle at a certain position r is given by the Smoluchowski equation [37]:

$$\frac{\partial p(\mathbf{r})}{\partial t} = \nabla \cdot \left[\frac{-p}{f_c} F + D \nabla p \right]$$ (16)

Here f_c is the friction constant and F is the thermal force acting on the particle due to the present of the temperature gradient. D is the Brownian diffusion coefficient. For stationary solution, the thermal force F is written as the following by introducing the definition of the Soret coefficient $S_T = D_T/D$:

$$F = -\frac{S_T}{\beta} \nabla T$$ (17)

Here D_T is the thermal diffusion coefficient or thermophoretic mobility, and $\beta = 1/k_B T$, k_B is Boltzmann's constant.

Strong temperature gradients can be induced around plasmonic nanostructures as a result of light energy absorption and heat dissipation to surrounding medium. Recently, the thermal
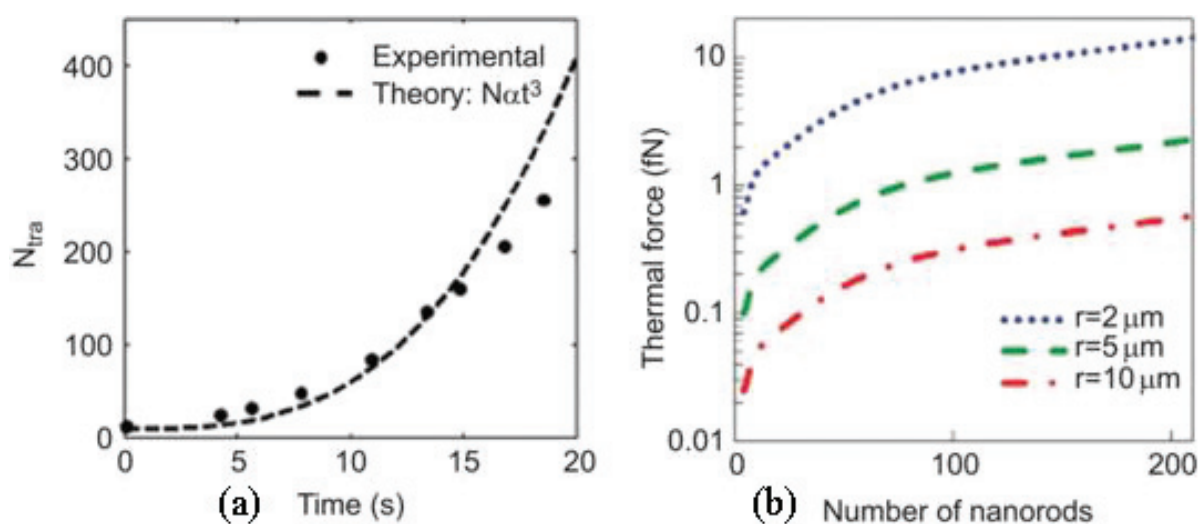

Figure 10. (a) Number of nanorods trapped in the focus as a function of the trapping time. (b) Opto-thermal force as a function of the number of nanorods trapped at different radii in the focal plane [38].

driving force induced by plasmonic resonances has been demonstrated in gold nanorods' solutions [38]. Experiments show that nanorods from a position up to 4–5 times the radius of the Airy spot of the laser beam can be attracted to the focal region. **Figure 10(a)** shows the dependence of the number of gold nanorods trapped in the focus as a function of trapping time. The trapped nanorods absorb a large amount of the energy from the trapping beam, which is converted to heating in the medium around the focal region and then to temperature increase in the surrounding medium. This opto-thermal process becomes significantly more pronounced when the number of trapped gold nanorods becomes large. The thermal attracting force arising from the temperature gradient can be large enough to overcome the Brownian motion of nanorods even at a distance several micrometres away from the focal spot, as shown in **Figure 10(b)**.

4. Conclusions

Resonant plasmonic structures allow for control of fundamental optical processes such as absorption and emission. By structuring metal surfaces on the subwavelength scale, plasmonic resonances can be designed to produce high-optical absorption in the broadband of wavelength. The absorbed optical energy is converted to heat, which can lead to significant local heating in metallic nanostructures and induce temperature gradient in the surrounding medium. The heat transfer between nanostructures is significantly enhanced by near field interaction. The thermal effects of plasmonic nanostructures can be used for energy conversion, optical trapping and thermal management.

Acknowledgements

Author details

Jingzhi Wu* and Yanhong Wang

*Address all correspondence to: jzwu@live.nuc.edu.cn

Laboratory of Nanophotonics, School of Information and Communications, North University of China, Taiyuan, Shanxi, China

References

[1] Halas NJ, Lal S, Chang WS, Link S, Nordlander P. Plasmons in Strongly Coupled Metallic Nanostructures. Chem Rev. 2011;111(6):3913–61.

[2]   Wang Y-H, Wu J, Wang G, Yang F. Resonance Modulation and Optical Force of Nanostructures with Au Slabs Array. Optik Int J Light Electron Optics. 2016;127(5):2969–72.

[3]   Kralik T, Hanzelka P, Zobac M, Musilova V, Fort T, Horak M. Strong Near-Field Enhancement of Radiative Heat Transfer Between Metallic Surfaces. Phys Rev Lett. 2012;109 (22):224302.

[4]   Li Z, Nan J, Zhang X, Ye S, Shen H, Wang S, et al. Modulate the Morphology and Spectroscopic Property of Gold Nanoparticle Arrays by Polymer-Assisted Thermal Treatment. J Phys Chem C. 2015;119(21):11839–45.

[5]   Wang H, Prasad Sivan V, Mitchell A, Rosengarten G, Phelan P, Wang L. Highly Efficient Selective Metamaterial Absorber for High-Temperature Solar Thermal Energy Harvesting. Sol Energy Mater Sol Cells. 2015;137:235–42.

[6]   Li W, Zhang L, Zhou J, Wu H. Well-Designed Metal Nanostructured Arrays for Label-Free Plasmonic Biosensing. J Mater Chem C. 2015;3(25):6479–92. doi:10.1039/C5TC00553A.

[7]   Fang Y, Jiao Y, Xiong K, Ogier R, Yang Z, Gao S, et al. Plasmon Enhanced Internal Photoemission in Antenna-Spacer-Mirror Based Au/TiO$_2$ Nanostructures. Nano Lett. 2015;15(6):4059–65.

[8]   Braun M, Wurger A, Cichos F. Trapping of Single Nano-objects in Dynamic Temperature Fields. Phys Chem Chem Phys. 2014;16(32):17343.

[9]   Wu JZ, Gan XS. Three Dimensional Nanoparticle Trapping Enhanced by Surface Plasmon Resonance. Opt Express. 2010;18(26):27619–26.

[10] Wu Y, Zhou L, Du X, Yang Y. Optical and Thermal Radiative Properties of Plasmonic Nanofluids Containing Core–Shell Composite Nanoparticles for Efficient Photothermal Conversion. Int J Heat Mass Transf. 2015;82:545–54.

[11] Coppens ZJ, Li W, Walker DG, Valentine JG. Probing and Controlling Photothermal Heat Generation in Plasmonic Nanostructures. Nano Lett. 2013;13(3):1023–8.

[12] Baffou G, Quidant R. Thermo-plasmonics: Using Metallic Nanostructures as Nano-sources of Heat. Laser Photon Rev. 2013;7(2):171–87.

[13] Chen Y, Nielsen TR, Gregersen N, Lodahl P, Mørk J. Finite-Element Modeling of Spontaneous Emission of a Quantum Emitter at Nanoscale Proximity to Plasmonic Waveguides. Phys Rev B. 2010;81(12):125431.

[14] Edalatpour S, Francoeur M. The Thermal Discrete Dipole Approximation (T-DDA) for Near-Field Radiative Heat Transfer Simulations in Three-Dimensional Arbitrary Geometries. J Quant Spectrosc Radiat Transf. 2014;133:364–73.

[15] Hohenester U. Quantum Corrected Model for Plasmonic Nanoparticles: A Boundary Element Method Implementation. Phys Rev B. 2015;91(20):205436.

[16] Lin W-C, Lin W-C, Tsai C-L, Lin K-P. Finite-Difference Time-Domain Simulation of Localized Surface Plasmon Resonance Adsorption by Gold Nanoparticles. In: Goh J, Lim CT,

editors. 7th WACBE World Congress on Bioengineering 2015: 6th to 8th July, 2015, Singapore. Cham: Springer International Publishing; 2015. pp. 138–41.

[17] Komarov PL, Burzo MG, Kaytaz G, Raad PE. Transient Thermo-reflectance Measurements of the Thermal Conductivity and Interface Resistance of Metallized Natural and Isotopically Pure Silicon. Microelectron J. 2003;34(12):1115–8.

[18] Smolin SY, Scafetta MD, Guglietta GW, Baxter JB, May SJ. Ultrafast Transient Reflectance of Epitaxial Semiconducting Perovskite Thin Films. Appl Phys Lett. 2014;105(2):22103.

[19] Suyuan B, Zhenan T, Zhengxing H, Jun Y, Jiaqi W. Thermal Conductivity Measurement of Submicron-Thick Aluminium Oxide Thin Films by a Transient Thermo-reflectance Technique. Chin Phys Lett. 2008;25(2):593–6.

[20] Wielgoszewski G, Gotszalk T. Chapter Four: Scanning Thermal Microscopy (SThM): How to Map Temperature and Thermal Properties at the Nanoscale. Adv Imag Elect Phys. 2015;190:177–221.

[21] Abou Nada F, Knappe C, Aldén M, Richter M. Improved Measurement Precision in Decay Time-Based Phosphor Thermometry. Appl Phys B. 2016;122(6):170.

[22] Bilde M, Barsanti K, Booth M, Cappa CD, Donahue NM, Emanuelsson EU, et al. Saturation Vapor Pressures and Transition Enthalpies of Low-Volatility Organic Molecules of Atmospheric Relevance: From Dicarboxylic Acids to Complex Mixtures. Chem Rev. 2015;115(10):4115–56.

[23] Zakaria I, Azmi WH, Mohamed WANW, Mamat R, Najafi G. Experimental Investigation of Thermal Conductivity and Electrical Conductivity of Al_2O_3 Nanofluid in Water: Ethylene Glycol Mixture for Proton Exchange Membrane Fuel Cell Application. Int Commun Heat Mass Transf. 2015;61:61–8.

[24] Reddy H, Guler U, Kildishev AV, Boltasseva A, Shalaev VM. Temperature-Dependent Optical Properties of Gold Thin Films. Opt Mater Express. 2016;6(9):2776–802.

[25] Shen P-T, Sivan Y, Lin C-W, Liu H-L, Chang C-W, Chu S-W. Temperature- and Roughness- Dependent Permittivity of Annealed/Unannealed Gold Films. Opt Express. 2016;24 (17):19254–63.

[26] Alabastri A, Tuccio S, Giugni A, Toma A, Liberale C, Das G, et al. Molding of Plasmonic Resonances in Metallic Nanostructures: Dependence of the Non-linear Electric Permittivity on System Size and Temperature. Materials. 2013;6(11):4879.

[27] Khodasevych IE, Wang L, Mitchell A, Rosengarten G. Micro- and Nanostructured Surfaces for Selective Solar Absorption. Adv Opt Mater. 2015;3(7):852–81.

[28] Cao F, McEnaney K, Chen G, Ren Z. A Review of Cermet-Based Spectrally Selective Solar Absorbers. Energy Environ Sci. 2014;7(5):1615–27. doi:10.1039/C3EE43825B.

[29] Mahdieh M, Badomi E. Determination of Roughness and Correlation Length of Dielectric Surfaces in Nano/Micro Scales Using Kirchhoff Approximation Method. J Opt. 2015;44 (3):240–248.

[30] Wang Y, Wu J. Broadband Absorption Enhancement of Refractory Plasmonic Material with Random Structure. Plasmonics. 2016:1–6.

[31] Orbanz P, Roy DM. Bayesian Models of Graphs, Arrays and Other Exchangeable Random Structures. IEEE Trans Pattern Anal Mach Intell. 2015;37(2):437–61.

[32] Boles YCAM. Thermodynamics: An Engineering Approach. 5th ed. Boston: McGraw-Hill;2006.

[33] Messina R, Tschikin M, Biehs S-A, Ben-Abdallah P. Fluctuation-Electrodynamic Theory and Dynamics of Heat Transfer in Systems of Multiple Dipoles. Phys Rev B. 2013;88 (10):104307.

[34] Baffou G, Kreuzer MP, Kulzer F, Quidant R. Temperature Mapping Near Plasmonic Nanostructures Using Fluorescence Polarization Anisotropy. Opt Express. 2009;17 (5):3291–8.

[35] Wang Y, Wu J. Radiative Heat Transfer Between Nanoparticles Enhanced by Intermediate Particle. AIP Adv. 2016;6(2):025104.

[36] Latella I, Pérez-Madrid A, Rubi JM, Biehs S-A, Ben-Abdallah P. Heat Engine Driven by Photon Tunneling in Many-Body Systems. Phys Rev Appl. 2015;4(1):011001.

[37] Wu J, Wang Y. Plasmonic Nanoparticle Trapping with Inhomogeneous Temperature Fields. Photon J IEEE. 2016;8(1):1–7.

[38] Gu M, Bao H, Gan X, Stokes N, Wu J. Tweezing and Manipulating Micro- and Nanoparticles by Optical Nonlinear Endoscopy. Light Sci Appl. 2014;3:e126.